Novel SBC@β-FeOOH Composites: Efficient Removal of Doxycycline in a Fixed-bed through Synergistic Adsorption and Heterogeneous Fenton-like Reaction

Xia Zhang [a], Bo Bai*[, b], Gianluca Li Puma [c], Honglun Wang [b], Yourui Suo [b]

[a] College of Environmental Science and Engineering, Chang'an University, Xi'an, 710054, P.R. China;

[b] Northwest Plateau Institute of Biology, Chinese Academy of Sciences, Xining, 810001, People's Republic of China;

[c] Environmental Nanocatalysis & Photoreaction Engineering, Department of Chemical Engineering, Loughborough University, Loughborough, LE11 3TU, United Kingdom.

* Corresponding author: Tel: +86 298 233 9052; Fax: +86 298 233 9961; Email: baibo@chd.edu.cn

Abstract: Akaganeite (β-FeOOH) nanoparticles were successfully anchored on the surface of porous sea buckthorn biocarbon (SBC) via a simple low-temperature hydrothermal process without use surfactants or external forces. The SBC@β-FeOOH composite was characterized by X-ray diffraction (XRD), scanning electron microscopy (SEM), and energy dispersive spectrometry (EDS). On the basis of characterization methods, a possible mechanism of formation of the SBC@β-FeOOH composite was discussed. The SBC@β-FeOOH composite was used in fixed-bed columns for the effective removal of doxycycline (DC) from an aqueous solution, by the synergistic effect of adsorption and Fenton-like oxidation reaction. The effects of inlet DC concentration (22-32 mg/L) feed flow rate (1-3 mL/min) SBC@β-FeOOH bed depth (0.7-1.5 cm) and pH (2-11) on the adsorption breakthrough profiles were investigated. The adsorption process was controlled by the ionic speciation of the adsorbate DC and the available binding sites of SBC@β-FeOOH. It was simulated by the Thomas and Yoon-Nelson models at different conditions. The bed of SBC@β-FeOOH saturated with DC was readily regenerated, in situ, by a heterogeneous Fenton-like oxidation reaction. The synergistic effect resulting from the biosorption nature of SBC and the catalytic oxidation properties of the supported β-FeOOH nanoparticles results in a new promising composite material for water treatment and purification.

Key Words: SBC@β-FeOOH; DC; Fixed-bed; Removal; Regeneration

1. Introduction

Adsorption using activated carbons is a widely used method to remove pollutants from water and wastewater [1-4]. However, the use of commercial activated carbons for water treatment can

be limited due to their relative high cost, especially in developing countries. In an effort to reduce the cost of the carbon sorbent material, the production of activated biocarbons from agricultural waste residues has attracted significant attention, also led by a sustainable utilization of natural carbon resources and the respect to the environment. For example, classical agricultural waste including rice husk [5], cocoa shell [6], peanut hull [7], trapa natans husk [8], grape stalk [9], cotton stalk [10] etc., have been extensively utilized for the preparation of activated biocarbon with a high adsorption capacity, substantial mechanical strength and low ash content [11]. Sea buckthorn is a thorny and branched deciduous shrub, 3-15 feet high, widely distributed in many countries including China, India, Pakistan, Nepal, Myanmar, Finland, Russia, Romania, Germany, Britain, and many other high altitude areas [12]. Nevertheless, sea buckthorn branches, as the by-product during the picking process of the fruit, have already given rise to environmental problems because of the chronic and casual disposal or incineration, which in turn may cause further water or air pollution. As a typical carbon-rich, cost-free and abundant agricultural solid waste, sea buckthorn branches offer a good natural source for the sustainable production of an effective activated biocarbon.

The treatment of contaminated water by heterogeneous Fenton oxidation with traditional slurry suspensions of iron oxide can be an expensive process since often large volumes of reagents (H_2O_2) and catalyst (Fe^{2+}) are needed, the water matrix usually consume inefficiently •OH radicals and in consequence, longer contact times are often required [13,14]. In contrast, the efficiency of the heterogeneous Fenton process for the treatment of wastewater can be increased significantly by applying an enrichment or pre-concentration sorption method prior to the oxidation of the contaminants by the Fenton process on the immobilized iron oxide [15,16]. For example, in our previous study the embedding of Fe_3O_4 nanoparticles onto the surface of yeast integrated the

61 biosorption features of yeast cells with the magnetic and Fenton catalytic properties of Fe_3O_4
62 nanoparticles, which was highly effective for the removal and oxidation of the cationic dye
63 methylene blue in water and wastewater [17]. The enhanced performance of this composite
64 catalyst can be attributed to the consecutive and synergistic effect of yeast biosorption and Fe_3O_4
65 nanoparticles heterogeneous Fenton oxidation/regeneration cycles.

66 Akaganeite, β-FeOOH, has been reported as a promising material for Fenton-like reactions in
67 heterogeneous systems, due to its large tunnel-type structure with iron atoms strongly bonded to
68 the framework [18-20]. Miyata et al. [21] reported that β-FeOOH was the most active among a
69 range of iron oxides and hydroxides (α-FeOOH, β-FeOOH, Fe_3O_4, α-Fe_2O_3 and γ-Fe_2O_3) for the
70 reduction of 4-nitrotoluene. Zhang et al. [22] developed TiO_2/β-FeOOH composite catalysts,
71 which exhibited excellent catalytic activity for the reduction of Cr(VI).

72 Inspired by this background, in this study we have assembled β-FeOOH nanoparticles onto
73 SBC activated biocarbons scaffolds through a simple hydrothermal process. Based on the XRD,
74 SEM, and EDS characterization methods, a possible formation mechanism of the SBC@β-FeOOH
75 composite was proposed. The adsorption and catalytic properties of the SBC@β-FeOOH were
76 investigated for the removal of doxycycline (DC), a common antibiotics compound used in human
77 therapy and the livestock industry [23-27], over a continuous, fixed-bed column system operated
78 in a cyclical manner of adsorption and regeneration. The breakthrough curves for the adsorption of
79 DC in the fixed-bed column were analyzed using mathematical models. The regeneration of the
80 saturated SBC@β-FeOOH composite sorbent was carried out by triggering the Fenton oxidation
81 reaction over the immobilized iron (β-FeOOH) by flowing an aqueous H_2O_2 solution. The
82 robustness of the materials over multiple loading and regeneration cycles makes it feasible for
83 practical environmental applications.

2. Materials and methods

2.1. Materials

The sea buckthorn branches used in this work were collected from Qinghai Province. Ferric chloride hexahydrate ($FeCl_3 \cdot 6H_2O$), urea (CON_2H_4), zinc chloride ($ZnCl_2$) and DC ($C_{22}H_{24}N_2O_8$) were provided by Xi'an Chemical Agent Corp. All chemicals used in this work were of analytical grade and used without further purification. Distilled water was used through all the experiments.

2.2. Fabrication of SBC@β-FeOOH

Sea buckthorn branches were impregnated with the activating agent $ZnCl_2$ in a 1/1 (w/w) (waste/$ZnCl_2$) ratio, for 24 h at room temperature. The material was then pyrolyzed in a tubular furnace at the temperature of 773 K for 1 h under N_2 atmosphere. The carbonized sample (SBC) was further washed with distilled water three times.

The SBC@β-FeOOH was prepared by a hydrothermal reaction process. In detail, 0.05 M $FeCl_3 \cdot 6H_2O$ and 0.2 M urea were firstly dissolved in distilled water at room temperature and under vigorous stirring to form a saffron yellow solution. Then, SBC was added to the saffron yellow solution and the color of the mixed solution changed to black. The mixture was transferred to a Teflon-lined stainless steel autoclave of 50 mL capacity and distilled water was added up to 80% of the total volume of the vessel. The vessel was sealed and maintained at 353 K for 6 h. The autoclave was then allowed to cool down to room temperature under ambient conditions. The resulting products were filtered, washed with distilled water, and finally dried under vacuum at 333 K for 6 h.

2.3. Characterizations of SBC@β-FeOOH

With the purpose of measuring the composition and phase purity of the samples, X-ray diffraction (XRD) were carried out on a Rigaku D/MAX-3C diffractometer operated at a voltage of 40 kV and a current of 20 mA at a 0.028 scan rate with Cu Ka radiation. Scanning electron microscopy (SEM) images were taken on a Tescan VEGA II LMH to determine the morphology of the SBC and SBC@β-FeOOH materials. The elemental distribution of iron, carbon, and oxygen in the SBC@β-FeOOH was evaluated using a multipoint energy-dispersive X-ray spectrometer (EDS; equipped with Hitachi S-2700 scanning electron microscope).

2.4. Adsorption tests

In order to investigate the synergistic effect of adsorption and the subsequent heterogeneous Fenton reaction, a fixed-bed column made of glass tube with an internal diameter of 0.6 cm and a length of 15 cm was packed with SBC@β-FeOOH and was operated in an up-flow mode. The effect of the influent DC concentration (22, 27 and 32 mg/L), flow rate (1, 2, and 3 mL/min), bed depth (0.7, 1.1 and 1.5 cm) and pH (2, 4, 6, 9, 11) on the column performance were investigated. Effluent samples from the column were collected at defined time intervals and analyzed by a Jenway 6405 UV−vis spectrophotometer at 351 nm.

The dynamic response and operation of the sorption column was evaluated by the analysis of the DC adsorption breakthrough profiles determined as the ratio C_t/C_0 vs t (min), where C_0 is the influent concentration, C_t is the effluent concentration, and t is the elapsed time. Q (mL/min) is the influent flow rate and t_{total} (min) is the total flow time.

The volume effluent V_{Eff} (mL) processed was determined as:

$$V_{\text{Eff}} = Q \cdot t_{\text{total}} \quad (1)$$

The total mass of DC adsorbed, q_{total} (mg), was estimated by the area described under the breakthrough curve:

$$q_{\text{total}} = \frac{Q}{1000} \int_{t=0}^{t=t_{\text{total}}} (C_0 - C_{\text{t}}) dt \quad (2)$$

The equilibrium uptake q_{e} (mg/g) was evaluated using Eq. (3) as the total amount of adsorbed (q_{total}) per gram of adsorbent m (g) when steady state conditions in the column were reached.

$$q_{\text{e}} = \frac{q_{\text{total}}}{m} \quad (3)$$

The total amount of DC fed to column m_{total} (mg) was calculated from Eq.(4):

$$m_{\text{total}} = \frac{C_0 \cdot Q \cdot t_{\text{total}}}{1000} \quad (4)$$

The empty bed contact time (EBCT) in the column, was evaluated by the ratio of the bed volume and the flow rate:

$$\text{EBCT(min)} = \frac{\text{bed volume (mL)}}{Q \text{ (mL/min)}} \quad (5)$$

2.5. Heterogeneous Fenton oxidation regeneration

The regeneration of the saturated sorbent in the bed was carried out by injecting an aqueous solution of H_2O_2 at a flow rate of 1 mL/min for 2 h, which triggered a Fenton-like oxidation reaction and the oxidation of the sorbed contaminants. The bed was then washed with distilled water, before the next loading cycle of a DC solution (27 mg/L) was flowed through the regenerated-bed column (1.1 bed depth) at a flow rate of 1 mL/min. After loading to the breakthrough point reaching saturation, the regeneration procedure was repeated as explained above.

3. Results and discussion

3.1. Characterization of SBC@β-FeOOH and formation mechanism

Fig. 1

The XRD patterns of the primitive SBC powder (trace a), the parallel β-FeOOH nanoparticles (trace b) and the SBC@β-FeOOH samples (trace c) are presented in Fig. 1, respectively. The broad diffraction peak around 2θ = 20° (trace a) indicates that the primitive SBC powder was of amorphous structure. The same shape was well established in other amorphous substance such as yeast-based activated biocarbon or commercially available activated carbon [28, 29]. The XRD pattern of the parallel β-FeOOH nanoparticles (trace b), matched the diffraction of tetragonal akaganeite (JCPDS card No. 34-1266) with cell constants of a = b =10.535 Å and c = 3.030 Å. Comparatively, the peaks of the as-prepared SBC@β-FeOOH species (trace c) were in agreement with the theoretical data of the tetragonal β-FeOOH phase. Since no further impurities peaks were detected, the successful loading of β-FeOOH on the SBC@β-FeOOH composites was confirmed.

Fig. 2

The formation of the β-FeOOH nanoparticles on the structure of SBC@β-FeOOH composites was further investigated by SEM analysis. Fig. 2a displays the morphology of the naked SBC powder, which has irregular shape with a large amount of pores on the surface. At higher magnification (Fig. 2b), the SBC abundant cavities with diverse diameters pervaded homogeneously on the surface of SBC, which contributed to the relatively large specific surface area of the SBC@β-FeOOH composites. Furthermore, the inset image in the bottom right corner of Fig. 2b demonstrated the longitudinal cross-section of the pores exhibiting a distinct tubular

shape. The loading of many β-FeOOH fine particles onto the SBC scaffold (Fig. 2c) led to a rough topographical surface of the SBC@β-FeOOH composite. The surface of the SBC was covered by small β-FeOOH nanoparticles, however, the porous structure of the parent SBC was maintained, which should favour the adsorption of contaminants. The occurrence of choked phenomenon for a few pore channels, in comparison with the original SBC substrate, provided assertive evidence that the β-FeOOH nanoparticles were anchored onto the surface of the SBC scaffold. Further, the absence of scattering particles around the composite material implied a strong adhesion between the SBC scaffold and the β-FeOOH nanoparticles. The higher magnification image in Fig. 2d shows β-FeOOH nanoparticle with an ellipsoidal morphology and smooth surface, resembling a 1D nanorods, 70-120 nm in width and 300-400 nm in length.

Fig. 3

The elemental composition of the composite was investigated by two-dimensional X-ray mapping of selected SBC@β-FeOOH zones (Fig. 3a). EDS analysis of SBC@β-FeOOH (the inset in the bottom left corner of Fig. 3a) showed that C, O, and Fe were the main elemental constituents, confirming the purity of the composite. The clear C, O and Fe elemental mapping images of SBC@β-FeOOH (Fig. 3b-d), indicated the homogeneous dispersions of C, O, and Fe on the surface of SBC substrate. More importantly, the elaborative observation of Fig. 3d confirmed that β-FeOOH nanoparticles were almost uniformly deposited on the SBC surface.

On the basis of XRD, SEM and EDS, a possible formation mechanism of β-FeOOH nanocrystals on the SBC substrate was proposed. The mechanism includes attachment, nucleation, growth and surface-regulation. Initially, minute β-FeOOH nanocrystals, assembled on the SBC, are gradually produced with an attachment process. The SBC possesses rough surfaces rich in hydroxyl group, and the bonding property of these functional groups on the ferric ions favors the

nucleation [30] of β-FeOOH on the SBC scaffold. The nucleation of nanocrystals is facilitated and energetically favoured, since the interfacial energy between the SBC and the β-FeOOH nanocrystal is smaller than the interfacial energy between the solution and the crystal. The granules formed at the early stage act as the cores for the further growth of β-FeOOH crystallites. With the adsorption to the ferric ions in β-FeOOH crystal nucleus, the epitaxial crystal growth takes place, at a suitable nucleating velocity, along the most favourable direction of crystallization from the nuclei, following a structure identified by a stack of O_3 and Fe layers: –Fe–Fe–O_3–Fe–Fe–O_3– [31]. The N–C=O groups of urea easily attach to the surface of the crystal faces gradually reducing the rate of growth of the crystal at the given crystallographic orientation [32], eventually blocking the further growth of these planes at later reaction times. In parallel, the subsequent nucleation and precipitation of β-FeOOH at an appropriately controlled rate and the anisotropic growth of the β-FeOOH nanocrystals, continues. This results in the growth of ellipsoid nanostructures. Finally, well-defined SBC@β-FeOOH composite materials are obtained with the rough surface assembled by β-FeOOH nanorods. The proposed mechanism was more explained by scheme reactions as follows:

$$CO(NH_2)_2+3H_2O \rightarrow CO_2+2NH_4OH$$

$$Fe^{3+}+3NH_4OH \rightarrow Fe(OH)_3+3NH_4^+$$

$$Fe(OH)_3 \rightarrow \beta\text{-}FeOOH+H_2O$$

3.2. Effects of operating conditions on DC adsorption in a fixed bed column

The performance of the SBC@β-FeOOH composite was evaluated in a fixed-bed column process operated for the sorption of DC from aqueous solutions. The use of a fixed-bed column process [33-36] allows more effective utilization of the absorbent capacity of the sorbent and

results in an effluent with higher quality [37]. In addition, in comparison with the batch method, the use of a fixed-bed column allows more effective cycles of adsorption/regeneration and reuse of the sorbent, and ultimately the scale-up of fixed-bed columns from the laboratory to pilot and industrial scale.

3.2.1. Effect of initial DC concentration, bed depths and flow rate

Fig. 4

The breakthrough profiles in Fig. 4a show that the breakthrough time decreased from 80 to 48 min when the concentration of DC of the influent varied from 22 to 32 mg/L in a bed of 1.1 cm in depth, operated at a flow rate of 1 mL/min and pH 6. These results are summarized in Table 1. The breakthrough curves were sharper at higher DC concentration, which suggested a relatively smaller depth of the mass-transfer zone and that intraparticle diffusion of the DC controlled the adsorption process. Equal observations have been reported for the biosorption of Cr (III) by olive stones [38] and in the removal of methylene blue by rice husk [39]. In addition, since the total amount of DC adsorbed decreased with increasing concentrations of DC in the influent, the diffusion process was concentration dependent.

The rate of accumulation of DC in the fixed-bed column is a function of the total mass of sorbent in the column. Fig. 4b show that the breakthrough time increased as the SBC@β-FeOOH bed depth varied from 0.7 to 1.5 cm, at a flow rate of 1.0 mL/min, an influent DC concentration of 27 mg/L and pH 6. The EBCT increased from 0.198 to 0.424 min as the bed depth was increased, which implies that the DC molecules could diffuse more effectively into the pore structure of the SBC@β-FeOOH with increased bed-depths. In this case, the mass-transfer zone formed moves further down the bed when bed depth increases, allowing a more effective contact between DC the

SBC@β-FeOOH in the column. On the other hand, the slope of the breakthrough curve reduced as the bed depth increased, which implies a broadening of the mass transfer zone. Obviously, the highest adsorption capacity occurred at the highest bed depth, since the total surface area of the adsorbent increased [40-42].

The breakthrough curves of DC at various flow rates from 1.0 to 3.0 mL/min with a bed depth of 1.1 cm, pH 6 and an initial DC concentration of 27 mg/L are shown in Fig. 4c. The breakthrough time decreased significantly with an increase in the flow rate, however, as the flow rate increased, much sharper breakthrough curves for DC adsorption onto SBC@β-FeOOH were observed. This results from a decrease in the contact time, which diminished the interaction of the DC solution with the SBC@β-FeOOH. In other words, at a lower flow rate DC had longer time to diffuse into the pores of the SBC@β-FeOOH and this resulted in a higher removal of DC in the column. Hence, breakthrough occurred later, resulting in higher bed adsorption capacity. Additionally, increasing the flow rate increases the rate of external mass transfer film thickness and resistance decreased by, leading to a higher overall mass transfer coefficient and adsorbate fluxes [43].

3.2.2. Effect of pH

The pH is an important factor that affects the sorption capacity of the sorbent. The pH has a significant effect of on the prevalent adsorption mechanisms and reflects the nature of the physico-chemical interaction of the compounds in solution and the binding sites of the sorbent [44]. Thus the pH of DC solution fed to the bed was fixed at 2.0, 4.0, 6.0, 9.0, and 11.0, while the influent DC concentration, flow rate and bed depth were kept constant at 27 mg/L, 1 mL/min, and 1.1 cm, respectively. The results presented in Figure 4(d) and Table 1shows that an increase in pH

of the feed solution decreases the volume of water treated until breakthrough of the bed occurred. In addition, as pH decreased, the breakthrough curves shifted to longer times removing more DC molecules. DC is an amphoteric molecule with multiple ionizable functional groups such as amino, phenol and alcohol at various pH values and has three pK_a values (3.5, 7.7 and 9.5), thus its predominant species are cation (DC^+) (below pH 3.5), due to the protonation of dimethyl-ammonium group, zwitterion (DC^0) (between pH 3.4 and 7.7), when the proton of phenolic diketone moiety is lost, and anion (DC^- and DC^{2-}, respectively, above pH 7.7 and 9.5), resulting from the loss of protons from the phenolic diketone moiety and tri-carbonyl system. For SBC@β-FeOOH, a low pH increased protonation, and this contributed to the diffusion of DC into the pores and generated a great deal of active sites on the surface of adsorbents [45]. Thus the increased adsorption capacity of DC at acidic condition results from the cationic character of DC [46]. DC^0 becomes predominant between pH 4 and 6, which decreases the electrostatic interatction with the sorbent and, therefore, the adsorption of DC through the surface of the SBC@β-FeOOH resulted in a shorter breakthrough time. When the pH is above 9, DC^0 begins to transform into DC^- and DC^{2-}. The decreased adsorption of DC results from the ionization of the surface oxygenated groups of the SBC at more alkaline pH, which results in higher negative surface charge density. Thus repulsive electrostatic forces can occur between the adsorbent and the DC molecules [47]. In brief, the anionic character of DC at higher pH and the adsorption performance of the bed decrease very rapidly with the pH increase. On the other hand, the lower adsorption amounts under alkaline conditions may result from the weak interaction of cation-π bonding and π-π stacking with SBC@β-FeOOH during the DC adsorption process [48].

Table 1

3.3. Adsorption columns modeling

The design and scale-up of fixed-bed adsorption columns requires the evaluation of the breakthrough curves of the effluent. Among many mathematical models that have been proposed for the design of fixed-bed adsorption systems, in this study we used the Thomas [49] and Yoon-Nelson [50] models, which are among the most widely and common methods.

3.3.1. Thomas model

The Thomas model estimates the dependence of solute concentration with time, in a fixed bed column, when internal and external mass transfer limitations are insignificant and in the absence of axial dispersion. The model has the following form:

$$\ln\left(\frac{C_0}{C_t}-1\right)=\frac{k_T q_0 m}{Q}-k_T C_0 t \quad (6)$$

where k_T is the Thomas rate constant (mL/min mg), m is the mass of adsorbent (g), q_0 is the equilibrium uptake capacity (mg/g) and Q is the flow rate (mL/min). C_0 and C_t are influent and the effluent concentrations (mg/L) of DC at any time t (min).

The adsorption capacity of the bed q_0 and the adsorption kinetic constant k_T were determined from a plot of $\ln[(C_0/C_t]$ against t at constant flow rate. The consistency of the experimental and predicted breakthrough curves of DC in the SBC@β-FeOOH fixed-bed columns was found to be satisfactory. A linear regression analysis of the experimental data and Eq. (6) were used to calculate the model parameters shown in Table 2. The regression coefficient (R^2) which ranged from 0.925 to 0.984 indicates that the Thomas model portrayed the column experimental data for the adsorption of DC very well. Moreover, the values of k_T decreased as the initial influent DC concentrations increased from 22 to 32 mg /L suggesting an increase of the effect of mass transfer

on the adsorption process. The highest k_T value at the lowest C_0 indicated that the adsorption of the DC was kinetically favorable at lower solute concentrations. The decrease of q_0 noted results from a decrease in the driving force for adsorption between the concentration of DC in the bulk and on the sorbent. Again, as the bed depth increased, the rate constant (k_T) decreased while the equilibrium uptake capacity (q_0) significantly increased. The values of k_T (mL/min•mg^{-1}) were 2.782, 6.267, and 12.467, respectively, with increasing flow rate of effluent while the values of q_0 decreased from 4.593 to 4.181. The increase of k_T value indicates the decrease of the mass-transport resistance and axial dispersion. And the decrease of q_0 is obvious as the adsorption capacity is directly proportional to the contact time. Thus, lower initial concentration, lower flow rate, and higher bed heights increase the rate of adsorption of DC in the SBC@β-FeOOH column.

3.3.2. Yoon-Nelson model

The Yoon-Nelson model is based on the assumption that the probability of adsorption onto the sorbent decreases as the fraction of solute being adsorbed decreases and as breakthrough is approached. The equation regarding to a single component system is expressed as:

$$\ln \frac{C_t}{C_0 - C_t} = k_Y t - \tau k_Y \quad (7)$$

where k_Y is the adsorption rate constant (min^{-1}), τ is the time to reach 50% of the adsorbate breakthrough (min) and t is the time (min).

Plotting $\ln[C_t/(C_0-C_t)]$ versus t determines the kinetic coefficient k_Y and τ through a linear fit of the experimental data, with slope of k_Y and intercept τk_Y. The Yoon-Nelson model sufficiently described the adsorption of DC on SBC@β-FeOOH in the fixed-bed columns. The R^2 values were higher than 0.925. The Yoon-Nelson model parameters were shown in Table 2. The times needed for 50% DC breakthrough from the experiments was in close agreement with the τ obtained from

the Yoon-Nelson model. The rate constant k_Y increased and the 50% breakthrough time τ decreased when both flow rate and DC inlet concentration increased. The values of τ increased and of k_Y decreased with increasing bed heights. Similar observations were made in sorption studies using granular activated carbon made from waste [51] and chitosan-clay [52].

Table 2

3.4. Heterogeneous Fenton oxidation in situ regeneration

Fig. 5

To exemplify the synergistic effect of adsorption and heterogeneous Fenton-like reaction, the DC-saturated beds were regenerated by H_2O_2. The small variation of the regeneration efficiency of the SBC@β-FeOOH beds regenerated with different H_2O_2 doses (Fig. 5) . As seen in Fig. 5, the regenerated SBC@β-FeOOH bed could attain a breakthrough time that coincided with that of fresh product.

$$H_2O_2\text{-regeneration efficiency}(\%)=\frac{t_{total}\text{ in the regenerated carbon}}{t_{total}\text{ in the fresh carbon}}\cdot 100\% \quad (8)$$

The regeneration efficiency of the saturated SBC@β-FeOOH using H_2O_2 (Eq. 8) was calculated as 78.1%, 90.6%, 65.6% and 56.3% for H_2O_2 concentrations in the feed of 3%, 5%, 10% and 15% (wt%), respectively. Obviously, the regeneration efficiency of the saturated SBC@β-FeOOH catalyst can be easily controlled by adjusting the H_2O_2 dosage. At low H_2O_2 dosage (e.g., 5%), the •OH and •OOH radicals generated by the Fenton-like reactions can attack the DC molecules easily [53], however, at higher H_2O_2 concentration such as 10% and 15% the scavenging of the radical species by H_2O_2 may become significant and hence the overall degradation efficiency of DC may decrease [53,54].

Scheme 1

The results demonstrated that flowing relatively low concentrations of aqueous H_2O_2 can efficiently restore the sorption capacity of saturated SBC@β-FeOOH columns. The regeneration performance of saturated SBC@β-FeOOH with 5% H_2O_2 in the fixed-bed column for three consecutive loading cycles is also shown in Fig. 5. The regeneration efficiency slightly decreased during the three consecutive cycles, which also coincided with a similar decrease of the adsorption capacity during the first and second absorption cycle. This might result from the stronger affinity of the intermediate products generated during the degradation process of DC. Despite this, the overall results support the idea that SBC@β-FeOOH composite integrates the biosorption features of SBC and catalytic properties of β-FeOOH nanoparticles, implying that the SBC@β-FeOOH can be used on multiple absorption cycles.

A schematic of the in-situ regeneration mechanism of the SBC@β-FeOOH composite is presented in Scheme 1. The regeneration processes might be ascribed to the synergistic effect, which works by the cooperation of biosorption merits of SBC and the heterogeneous catalytic oxidation properties of the supported β-FeOOH nanoparticles. More specifically, the DC molecules can be transferred from the aqueous solution to the SBC by sorption and pre-concentrated on the bare areas of the SBC@β-FeOOH composite. Then, the adsorbed DC molecules can be oxidized by the heterogeneous β-FeOOH/H_2O_2 Fenton-like oxidation reaction by switching to a flow of an H_2O_2 in water which generated radical species [55-57]. Firstly, SBC≡Fe^{3+} is reduced to SBC≡Fe^{2+} by H_2O_2, generating •OOH. Secondly, the SBC≡Fe^{2+} produced reacts with another molecule of H_2O_2, producing hydroxyl anion and •OH radical. In addition, the combination of H_2O_2/SBC≡Fe^{3+} produced SBC≡Fe^{2+} and •OOH radical followed by the reoxidation of SBC≡Fe^{2+} by H_2O_2. Therefore, DC molecules can be oxidized by the combined action of •OH and •OOH, and the adsorbed DC molecules on the surface of SBC@β-FeOOH

composite were removed completely. In consequence, the saturated adsorption sites on the surface of SBC@β-FeOOH composite could be easily regenerated. Compared with other types of adsorbent, such as activated carbon samples with ferric nitrate[46], magnetic porous carbon with maghemite[48] graphene-like layered molybdenum disulfide [58] and montmorillonite[59], the most obvious advantage of SBC@β-FeOOH is its regeneration capacity which was structured by heterogeneous Fenton-like oxidation in the treating process of doxycycline.

4. Conclusion

A novel and low-cost composite material SBC@β-FeOOH, which integrates the biosorption features of SBC and catalytic properties of β-FeOOH nanoparticles, was synthesized in one step via a hydrothermal process. The SBC@β-FeOOH proved to be a promising and effective composite material for the removal and the oxidative destruction of DC from aqueous solution performed in a fixed-bed column study. The adsorption of DC on SBC@β-FeOOH bed was found to be depended on the influent concentration, flow rate, bed depth and pH. The SBC@β-FeOOH adsorbent was suitable for the adsorption of DC at acidic, neutral and mildly alkaline pH, with the highest performance observed at acidic pH. The adsorption process was controlled by the ionic speciation of the adsorbate DC and the available binding sites of SBC@β-FeOOH. Under the experimental condition, the column experimental data were analyzed by the Thomas and Yoon-Nelson models. H_2O_2-based heterogeneous Fenton oxidation proved to be a viable and efficient process for the in situ regeneration of SBC@β-FeOOH saturated beds. The results demonstrate that the sea buckthorn branches are a potential material for the preparation of SBC. Considering the facile method of fabrication of the composite from abundant and low cost agricultural wastes, the superior adsorption performance, the simple and effective way of

regeneration and the robustness of the adsorbent for consecutive adsorption/regeneration cycles, we conclude that the SBC@β-FeOOH composite should be a promising and practical adsorbent for removal and destruction of organic compounds in wastewater. The embedding of β-FeOOH onto the SBC surface can be extended to the simple fabrication of other β-FeOOH nanoparticles/agricultural wastes materials.

Acknowledgments

This work was supported by Shaanxi Provincial Natural Science Foundation of China (No.2015JM2071), National Natural Science Foundation of China (No.21176031) and Fundamental Research Funds for the Central Universities (No. 2014G3292007).

References

[1] L. Ji, W. Chen, S. Zheng, Z. Xu, D. Zhu, Adsorption of sulfonamide antibiotics to multi-walled carbon nanotubes, Langmuir 25 (2009) 11608-11613.

[2] Y. Gao, Y. Li, L. Zhang, H. Huang, J.-J. Hu, S.M. Shah, X.-G. Su, Adsorption and removal of tetracycline antibiotics from aqueous solution by graphene oxide, J. Colloid Interface Sci. 368 (2012) 540-546.

[3] N.K. Amin, Removal of direct blue-106 dye from aqueous solution using new activated carbons developed from pomegranate peel: adsorption equilibriumand kinetics, J. Hazard. Mater. 165 (2009) 52-62.

[4] S. Noreen, H.N. Bhatti, S. Nausheen, S. Sadaf, M. Ashfaq, Batch and fixed bed adsorption study for the removal of Drimarine Black CL-B dye from aqueous solution using a lignocellulosic waste: a cost affective adsorbent, Ind. Crop. Prod. 50 (2013) 568-579.

[5] L.-L. Ding, B. Zou, W. Gao, Q. Liu, Z.-C. Wang, Y.-P. Guo, X.-F. Wang, Y.-H. Liu, Adsorption of Rhodamine-B from aqueous solution using treated rice husk-based activated carbon, Colloids Surf., A 446 (2014) 1-7.

[6] M.C. Ribas, M.A. Adebayo, L.D.T. Prola, E.C. Lima, R. Cataluña, L.A. Feris, M.J. Puchana-Rosero, F.M. Machado, F.A. Pavan, T. Calvete, Comparison of a homemade cocoa shell activated carbon with commercial activated carbon for the removal of reactive violet 5 dye from aqueous solutions, Chem. Eng. J. 248 (2014) 315-326.

[7] R.-M. Gong, Y. Ding, M. Li, C. Yang, H.-J. Liu, Y.-Z. Sun, Utilization of powdered peanut hull as biosorbent for removal of anionic dyes from aqueous solution, Dyes Pigments 64 (2005) 187-192.

[8] W.-F. Liu, J. Zhang, C.-L. Zhang, Y.-F. Wang, Y. Li, Adsorptive removal of Cr (VI) by Fe-modified activated carbon prepared from Trapa natans husk, Chem. Eng. J. 162 (2010) 677-684.

[9] I. Ozdemir, M. Şahin, R. Orhan, M. Erdem, Preparation and characterization of activated carbon from grape

stalk by zinc chloride activation, Fuel Process. Technol. 125 (2014) 200-206.

[10] H. Deng, L. Yang, G.-H. Tao, J.-L. Dai, Preparation and characterization of activated carbon from cotton stalk by microwave assisted chemical activation-application in methylene blue adsorption from aqueous solution, J. Hazard. Mater. 166 (2009) 1514-1521.

[11] D. Savova, E. Apak, E. Ekinci, F. Yardim, N. Petrov, T. Budinova, M. Razvigorova, V. Minkova, Biomass conversion to carbon adsorbents and gas, Biomass and Bioenergy 21 (2001) 133-142.

[12] L. D. Kagliwal, S.C. Patil, A.S. Pol, R. S. Singhal, V. B. Patravale, Separation of bioactives from seabuckthorn seeds by supercritical carbon dioxide extraction methodology through solubility parameter approach, Sep. Purif. Technol. 80 (2011) 533-540.

[13] M. Aleksić, H. Kušić, N. Koprivanac, D. Leszczynska, A. Lončarić Božić, Heterogeneous Fenton type processes for the degradation of organic dye pollutant in water-The application of zeolite assisted AOPs, Desalination. 257 (2010) 22-29.

[14] W.-G. Li, Y. Wang, A. Irini, Effect of pH and H_2O_2 dosage on catechol oxidation in nano-Fe_3O_4 catalyzing UV-Fenton and identification of reactive oxygen species, Chem. Eng. J. 244 (2014) 1-8.

[15] Y. Li, F.-S. Zhang, Catalytic oxidation of Methyl Orange by an amorphous FeOOH catalyst developed from a high iron-containing fly ash, Chem. Eng. J. 158 (2010) 148-153.

[16] M.Gonçalves, M.C. Guerreiro, L.C.A. de Oliveira, C.S. de Castro, A friendly environmental material: Iron oxide dispersed over activated carbon from coffee husk for organic pollutants removal, J. Environ. Manage. 127 (2013) 206-211.

[17] R. Song, B. Bai, G.L. Puma, H.-L. Wang, Y.-R. Suo, Biosorption of azo dyes by raspberry-like Fe_3O_4@yeast magnetic microspheres and their efficient regeneration using heterogeneous fenton-like catalytic processes over an up-flow packed reactor, React. Kinet. Mech. Cat. DOI 10.1007/s11144-015-0854-z

[18] L.-Y. Zhang, J. Feng, D.-S. Xue, An investigation of thermal decomposition of β-FeOOH nanowire arrays

assembled in AAO templates, Mater. Lett. 61 (2007) 1363-1367.

[19] C.-Z. Wei, Z.-D. Nan, Effects of experimental conditions on one-dimensional single-crystal nanostructure of β-FeOOH, Mater. Chem. Phys. 127 (2011) 220-226.

[20] E.A. Deliyanni, D.N. Bakoyannakis, A.I. Zouboulis, K.A. Matis, L. Nalbandian, Akaganéite-type β-FeO (OH) nanocrystals: preparation and characterization, Microporous Mesoporous Mater. 42 (2001) 49-57.

[21] T. Miyata, Y. Ishino, T. Hirashima, Catalytic reduction of aromatic nitro compounds with hydrazine hydrate in the presence of Iron (III) oxide hydroxide, Synthesis 11(1978): 834-835.

[22] M. Zhang, Z. Xu, J. Liang, L. Zhou, C. Zhang. Potential application of novel TiO_2/β-FeOOH composites for photocatalytic reduction of Cr(VI) with an analysis of statistical approach, Int. J. Environ. Sci. Te. DOI 10.1007/s13762-014-0533-z.

[23] C. Zhao, M. Pelaez, X. Duan, H. Deng, K. O'Shea, D. Fatta-Kassinos, D. D. Dionysiou, Role of pH on photolytic and photocatalytic degradation of antibiotic oxytetracycline in aqueous solution under visible/solar light: Kinetics and mechanism studies, Appl. Catal., B- Environ. 134-135 (2013) 83-92.

[24] Y. Gao, Y. Li, L. Zhang, H. Huang, J.-J. Hu, S.M. Shah, X.-G. Su, Adsorption and removal of tetracycline antibiotics from aqueous solution by graphene oxide, J. Colloid Interf. Sci. 368 (2012) 540-546.

[25] M. Ghaemi, G. Absalan, Fast removal and determination of doxycycline in water samples and honey by Fe_3O_4 magnetic nanoparticles, J. Iran. Chem. Soc. 12 (2015)1-7.

[26] M. Erşan, E. Bağda, E. Bağda. Investigation of kinetic and thermodynamic characteristics of removal of tetracycline with sponge like, tannin based cryogels, Colloids Surf., B. 104 (2013) 75-82.

[27] S. Zaidi, T. Chaabane, V. Sivasankar, A. Darchen, R. Maachi, T.A.M. Msagati, Electro-coagulation coupled electro-flotation process: Feasible choice in doxycycline removal from pharmaceutical effluents, Arabian J. Chem. DOI 10.1016/j.arabjc.2015.06.009

[28] R. Nacco, E. Aquarone, Preparation of active carbon from yeast, Carbon 16 (1978)31-34

[29] Z. C. Kadirova, K. Katsumata, T. Isobe, N. Matsushita, A. Nakajima, K. Okada, Adsorption and photodegradation of methylene blue with Fe_2O_3-activated carbons under UV illumination in oxalate solution, J. Environ. Chem. Eng. 2 (2014) 2026-2036.

[30] Z.-G. An, J.-J. Zhang, S.-L. Pan, Synthesis and controlled assembly of α-FeOOH and α-Fe_2O_3 nanobelt arrays on hollow glass spheres, Mater. Res. Bull. 47 (2012) 3976-3982.

[31] H.-J. Song, X.-Q. Zhang, T. Chen, X.-H. Jia, One-pot synthesisofbundle-like β-FeOOH nanorods and their transformation to porous α-Fe_2O_3 microspheres, Ceram. Int. 40 (2014) 15595-15602.

[32] H.-F. Liang, B.-B. Xu, Z.C.Wang, Self-assembled 3D flower-like α-Fe_2O_3 microstructures and their superior capability for heavy metal ion removal, Mater. Chem. Phys. 141(2013)727-734.

[33] M. Izquierdo, C. Gabaldón, P. Marzal, F.J. álvarez-Hornos, Modeling of copper fixed-bed biosorption from wastewater by Posidonia oceanica, Bioresource Technol. 101 (2010) 510-517.

[34] E. Oguz, M. Ersoy, Biosorption of cobalt(II) with sunflower biomass from aqueous solutions in a fixed bed column and neural networks modelling, Ecotox. Environ. Safe. 99(2014)54-60.

[35] E. Malkoc, Y. Nuhoglu, Removal of Ni(II) ions from aqueous solutions using waste of tea factory: Adsorption on a fixed-bed column, J. Hazard. Mater. 135 (2006) 328-336.

[36] A.C. Texier, Y. Andr`es, C.F. Brasquet, P.I. Cloirec, Fixed-bed study for lanthanide (La Eu, Yb) ions removal from aqueous solutions by immobilized Pseudomonas aeruginosa: experimental data and modelization, Chemosphere 47 (2002) 333-342.

[37] R. Senthilkumar, K. Vijayaraghavan, M. Thilakavathi, P.V.R. Iyer, M. Velan, Seaweeds for the remediation of wastewaters contaminated with zinc(II) ions, J. Hazard. Mater. 136 (2006) 791-799.

[38] M. Calero, F. Hernáinz, G. Blázquez, G. Tenorio, M.A. Martín-Lara, Study of Cr (III) biosorption in a fixed-bed column, J. Hazard. Mater. 171 (2009) 886-893.

[39] R.-P. Han, Y.-F. Wang, W.-H. Yu, W.-H. Zou, J. Shi, H.-M. Liu, Biosorption of methylene blue from

aqueous solution by rice husk in a fixed-bed column, J. Hazard. Mater. 141 (2007) 713-718.

[40] P.D. Saha, S. Chakraborty, S. Chowdhury, Batch and continuous (fixed-bed column) biosorption of crystal violet by Artocarpus heterophyllus (jackfruit) leaf powder, Colloid. Surface. B 92 (2012) 262-270.

[41] J. Wu, H.-Q. Yu, Biosorption of 2,4-dichlorophenol from aqueous solutions by immobilized Phanerochaete chrysosporium biomass in a fixed-bed column, Chem. Eng. J. 138 (2008) 128-135.

[42] J. Cruz-Olivares, C. Pérez-Alonso, C. Barrera-Díaz, F. Ureña-Nuñez, M.C. Chaparro-Mercado, B. Bilyeu, Modeling of lead (II) biosorption by residue of allspice in a fixed-bed column, Chem. Eng. J. 228 (2013) 21-27.

[43] S. Chen, Q. Yue, B. Gao, Q. Li, X. Xu, K. Fu, Adsorption of hexavalent chromium from aqueous solution by modified corn stalk: a fixed-bed column study, Bioresource technol. 113 (2012) 114-120.

[44] Z. Aksu, F. G¨onen, Biosorption of phenol by immobilized activated sludge in a continuous packed bed: prediction of breakthrough curves, Process Biochem. 39 (2004) 599-613.

[45] R. Jain, M. Mathur, S. Sikarwar, A. Mittal, Removal of the hazardous dyerhodamine B through photocatalytic and adsorption treatments, J. Environ. Manage. 85 (2007) 956-964.

[46] G. Li, D.-S. Zhang, M. Wang, J. Huang, L.-H. Huang, Preparation of activated carbons from Iris tectorum employingferric nitrate as dopant for removal of tetracycline from aqueous solutions, Ecotox. Environ. Safe. 98(2013)273-282.

[47] J. Rivera-Utrilla, C.V. Gómez-Pacheco, M. Sánchez-Polo, J.J. López-Peñalver, R. Ocampo-Pérez, Tetracycline removal from water by adsorption/bioadsorption on activated carbons and sludge-derived adsorbents, J. Environ. Manage. 131 (2013) 16-24.

[48] X.-D. Zhu, Y.-C. Liu, F. Qian, C. Zhou, S.-C. Zhang, J.-M. Chen, Preparation of magnetic porous carbon from waste hydrochar by simultaneous activation and magnetization for tetracycline removal, Bioresource Technol. 154 (2014) 209-214.

513 [49] H.C. Thomas, Heterogeneous ion exchange in a flowing system, J. Am. Chem. Soc. 66 (1944) 1664-1666.

514 [50] Y.H. Yoon, J.H. Nelson, Application of gas adsorption kinetics I. A theoretical model for respirator cartridge
515 service life, Am. Ind. Hyg. Assoc. J. 45 (1984) 509-516.

516 [51] A.A. Ahmad, B.H. Hameed, Fixed-bed adsorption of reactive azo dye onto granular activated carbon
517 prepared from waste, J. Hazard. Mater. 175 (2010) 298-303.

518 [52] M. Auta, B.H. Hameed, Chitosan-clay composite as highly effective and low-cost adsorbent for batch and
519 fixed-bed adsorption of methylene blue, Chem. Eng. J. 237 (2014) 352-361.

520 [53] X.-Y. Li, Y. Huang, C. Li, J.-M. Shen, Y. Deng, Degradation of pCNB by Fenton like process using
521 α-FeOOH, Chem. Eng. J. 260 (2015) 28-36.

522 [54] W. Wang, Y. Liu, T.-L. Li, M.-H. Zhou, Heterogeneous Fenton catalytic degradation of phenol based on
523 controlled release of magnetic nanoparticles, Chem. Eng. J. 242 (2014) 1-9.

524 [55] L.C.A. Oliveira, M. Goncalves, M.C. Guerreiro, T.C. Ramalho, J.D. Fabris, M.C. Pereira, K. Sapag, A new
525 catalyst material based on niobia/iron oxide composite on the oxidation of organic contaminants in water via
526 heterogeneous Fenton mechanisms, Appl. Catal., A-Gen. 316 (2007) 117-124.

527 [56] R.C.C. Costa, M.F.F. Lelis, L.C.A. Oliveira, J.D. Fabris, J.D. Ardisson, R.R.V.A. Rios, R.M. Lago, Novel
528 active heterogeneous Fenton system based on $Fe_{3-x}M_xO_4$ (Fe, Co, Mn, Ni): the role of M^{2+} species on the
529 reactivity towards H_2O_2 reactions, J. Hazard. Mater. 129 (2006), 171-178.

530 [57] L.C.A. Oliveira, M. Goncalves, M.C. Guerreiro, T.C. Ramalho, J.D. Fabris, M.C. Pereira, K. Sapag, A new
531 catalyst material based on niobia/iron oxide composite on the oxidation of organic contaminants in water via
532 heterogeneous Fenton mechanisms, Appl. Catal., A-Gen 316 (2007) 117-124.

533 [58] Y.-H. Chao, W.-S. Zhu, X.-Y. Wu, F.-F. Hou, S.-H. Xun, P.-W. Wu, H.-Y. Ji, H. Xu, H.-M. Li, Application of
534 graphene-like layered molybdenum disulfide and its excellent adsorption behavior for doxycycline
535 antibiotic, Chem. Eng. J. 243 (2014) 60-67.

[59] M.E. Parolo, M.C. Savini, J.M. Vallés, M.T. Baschini, M.J. Avena, Tetracycline adsorption on montmorillonite: pH and ionic strength effects, Appl. Clay Sci. 40(2008)179-186.

Table captions

Table 1. Parameters in fixed-bed column for DC adsorption by SBC@β-FeOOH.

Table 2. Parameters of Thomas and Adams-Bohart models for DC adsorption by SBC@β-FeOOH.

.

Table 1.

C_0 (mg/L)	Z (cm)	Q (mL/min)	pH	t_{total} (min)	m_{total} (mg)	q_{total} (mg)	q_e (mg/g)	V_{Eff} (mL)	EBCT (min)
22	1.1	1	6	80	1.760	0.593	7.409	80	0.311
27	1.1	1	6	64	1.728	0.459	5.734	64	0.311
32	1.1	1	6	48	1.536	0.385	4.816	48	0.311
27	0.7	1	6	44	1.188	0.264	5.286	44	0.198
27	1.1	1	6	64	1.728	0.459	5.734	64	0.311
27	1.5	1	6	88	2.376	0.744	6.767	88	0.424
27	1.1	1	6	64	1.728	0.459	5.734	64	0.311
27	1.1	2	6	31	1.674	0.456	5.703	62	0.156
27	1.1	3	6	18	1.458	0.448	5.597	54	0.104
27	1.1	1	2	108	2.916	1.072	13.403	108	0.311
27	1.1	1	4	84	2.268	0.753	9.408	84	0.311
27	1.1	1	6	64	1.728	0.459	5.734	64	0.311
27	1.1	1	9	52	1.404	0.302	3.773	52	0.311
27	1.1	1	11	32	0.864	0.203	2.533	32	0.311

Table 2.

C_0 (mg/L)	Z (cm)	Q (mL/min)	pH	Thomas model			Yoon & Nelson model		
				$k_T \times 10^{-3}$ mL/min·mg	q_0 mg/g	R^2	K_Y min^{-1}	τ min	R^2
22	1.1	1	6	2.785	7.111	0.9435	0.061	25.97	0.9435
27	1.1	1	6	2.782	4.593	0.9404	0.075	13.63	0.9404
32	1.1	1	6	3.316	3.438	0.9837	0.106	8.60	0.9837
27	0.7	1	6	4.000	2.839	0.9675	0.108	5.26	0.9675
27	1.1	1	6	2.782	4.593	0.9404	0.075	13.63	0.9404
27	1.5	1	6	2.341	6.810	0.9253	0.063	27.83	0.9253
27	1.1	1	6	2.782	4.593	0.9404	0.075	13.63	0.9404
27	1.1	2	6	6.267	4.393	0.9359	0.169	6.51	0.9359
27	1.1	3	6	12.467	4.181	0.9620	0.337	4.13	0.9620
27	1.1	1	2	2.337	15.103	0.9142	0.063	44.75	0.9142
27	1.1	1	4	2.503	9.783	0.9163	0.068	28.98	0.9163
27	1.1	1	6	2.782	4.593	0.9404	0.075	13.63	0.9404
27	1.1	1	9	3.363	1.975	0.9275	0.091	5.85	0.9275
27	1.1	1	11	6.241	1.657	0.9846	0.169	4.91	0.9846

Figure captions

Figure1. XRD pattern of (a) the original SBC powder, (b) parallelβ-FeOOH nanoparticles and (c) SBC@β-FeOOH samples.

Figure 2. SEM images of (a) overall morphology of original SBC powder, (b) SBC observed under higher magnification, (c) the SBC@β-FeOOH products, and (d) an enlarged image of SBC@β-FeOOH under greater magnification.

Figure 3. Selected zones of SBC@β-FeOOH samples (a) and corresponding X-Ray mapping (b) for C, (c) O, and (d) Fe elements.

Figure 4. Effect of (a) initial DC concentration (Z = 1.1 cm, *Q*=1.0 mL/min, pH=6), (b) bed depths (C_0 = 27 mg /L, *Q*=1.0 mL/min, pH=6) (c) flow rate (Z = 1.1 cm, C_0 = 27 mg /L, pH=6) and pH (Z = 1.1 cm, *Q*=1.0 mL/min, C_0 = 27 mg /L) on breakthrough curve.

Figure 5. Schematic of the in-situ regeneration mechanisms (a) and breakthrough time of the regenerated SBC@β-FeOOH at various H_2O_2 concentration compared with fresh (b) products.

Scheme 1 Formation mechanisms for the SBC@β-FeOOH composite and their synergetic effect in the removal of DC aqueous solution.

Figure 1.

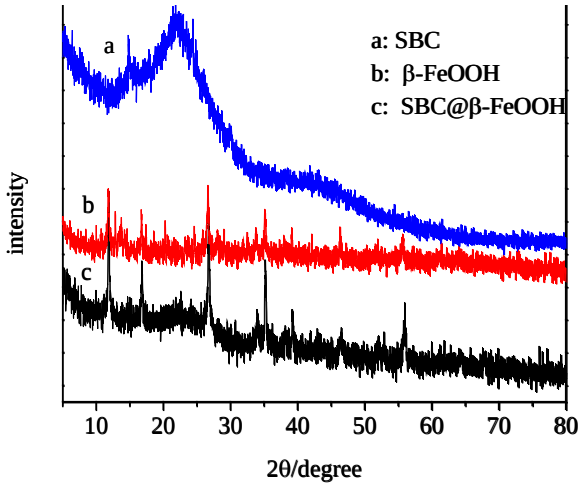
a: SBC
b: β-FeOOH
c: SBC@β-FeOOH
a
b
c
intensity
10
20
30
40
50
60
70
80
2θ/degree

Figure 2.

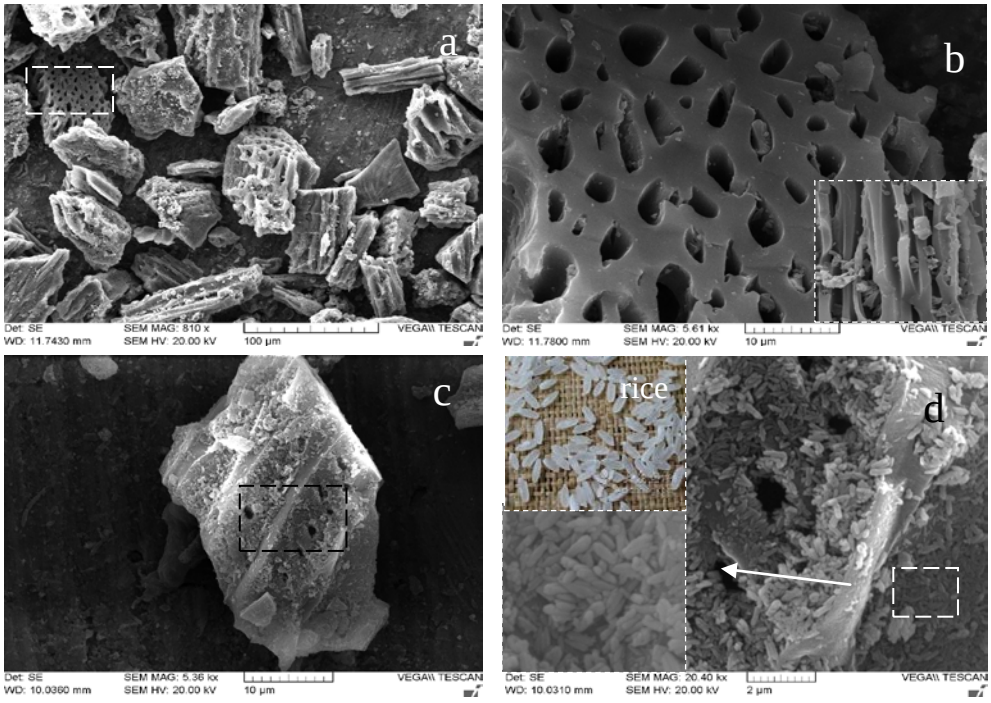
a
Det: SE
WD: 11.7430 mm
SEM MAG: 810 x
SEM HV: 20.00 kV
100 µm
VEGA\\ TESCAN
b
Det: SE
WD: 11.7800 mm
SEM MAG: 5.61 kx
SEM HV: 20.00 kV
10 µm
VEGA\\ TESCAN
c
Det: SE
WD: 10.0360 mm
SEM MAG: 5.36 kx
SEM HV: 20.00 kV
10 µm
VEGA\\ TESCAN
rice
d
Det: SE
WD: 10.0310 mm
SEM MAG: 20.40 kx
SEM HV: 20.00 kV
2 µm
VEGA\\ TESCAN

Figure 3.

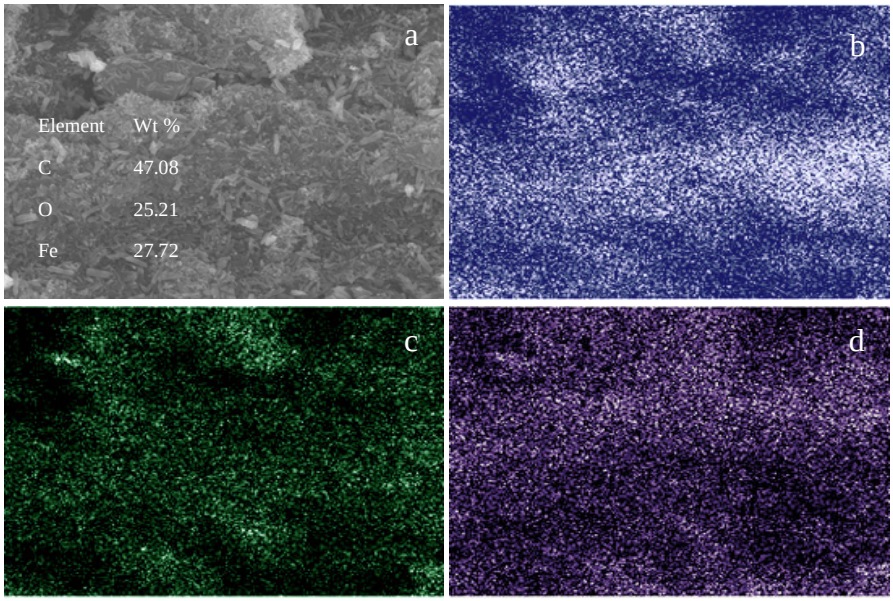

Figure 4.

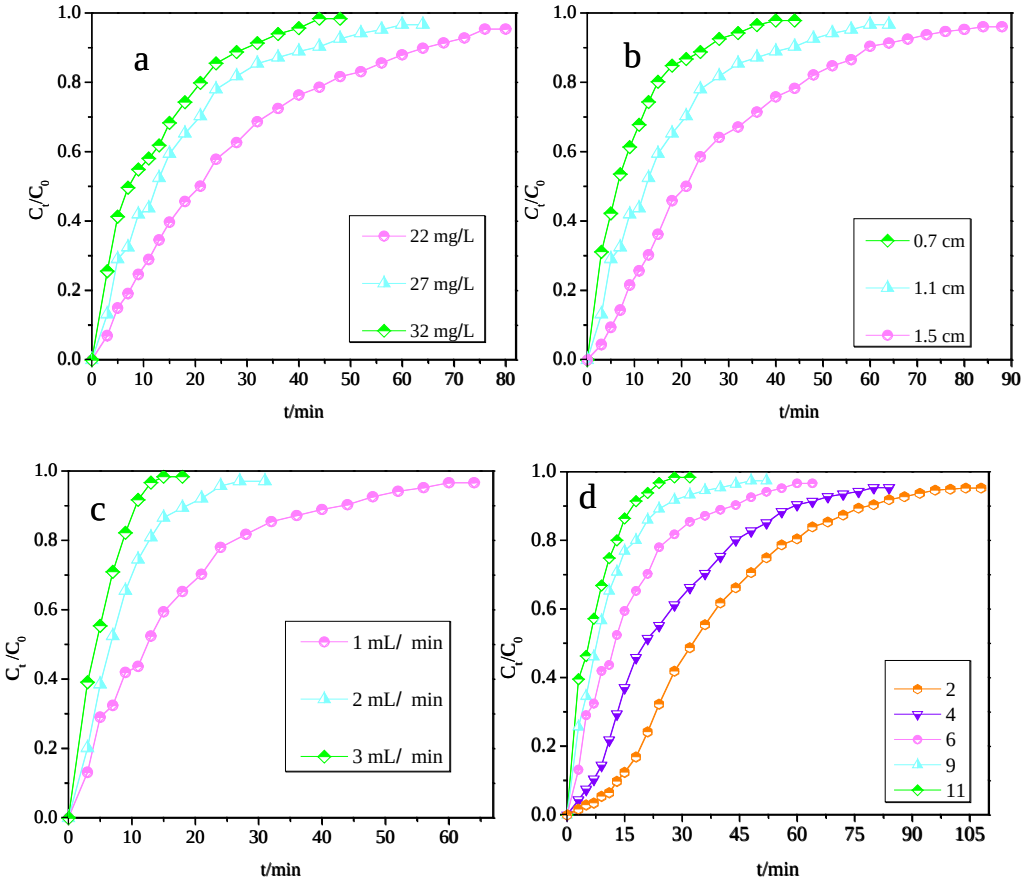
a
b
c
d
C_t/C_0
t/min
22 mg/L
27 mg/L
32 mg/L
0.7 cm
1.1 cm
1.5 cm
1 mL/ min
2 mL/ min
3 mL/ min
2
4
6
9
11

Figure 5.

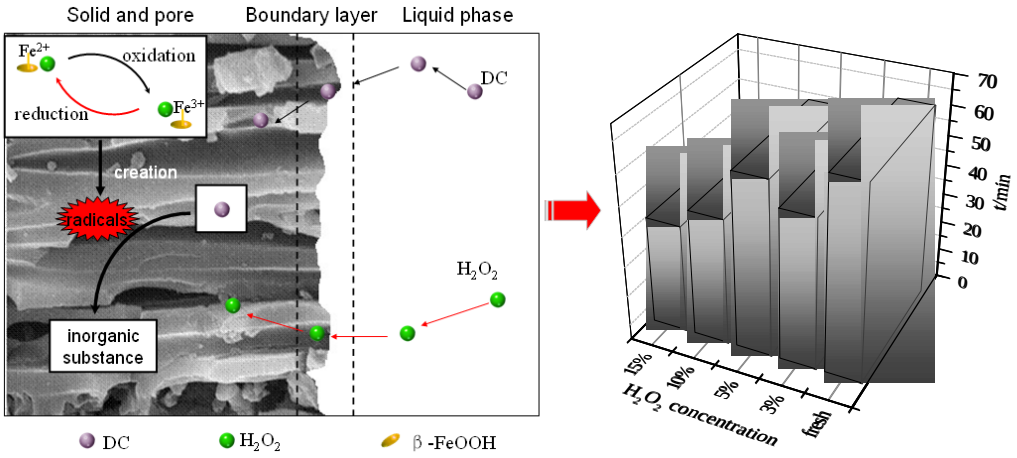

Scheme 1

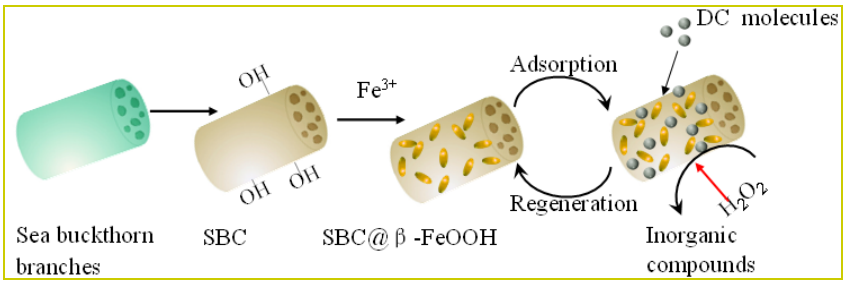
DC molecules
Adsorption
OH
OH
OH
Fe3+
Regeneration
H2O2
Sea buckthorn branches
SBC
SBC@ β -FeOOH
Inorganic compounds